Heterogeneous Kinetics of Metal- and Ligand-Based Redox Reactions within Adsorbed Monolayers

Robert J. Forster

School of Chemical Sciences, Dublin City University, Dublin 9, Ireland

Received October 18, 1995[⊗]

Dense monolayers of $[Os(bpy)_2py(p3p)]^{2+}$, where bpy is 2,2′-bipyridyl, py is pyridine, and p3p is 4,4′-trimethylenedipyridine, have been formed by spontaneous adsorption onto clean platinum microelectrodes. Three well-defined waves, corresponding to osmium- and bipyridyl-based redox reactions, are observed in cyclic voltammetry of these monolayers, where the supporting electrolyte is tetrabutylammonium tetrafluoroborate ($TBABF_4$) dissolved in acetonitrile. These reactions correspond to the charge states 3+/2+, 2+/1+, and 1+/0, respectively. Chronoamperometry, conducted on a microsecond time scale, has been used to measure the heterogeneous electron transfer rate constant, k/s^{-1}, for all three redox processes. For concentrations of $TBABF_4$ above 0.1 M, heterogeneous electron transfer is characterized by a single unimolecular rate constant. Standard heterogeneous electron transfer rate constants, $k°$, have been evaluated by extrapolating Tafel plots of ln k vs overpotential, η, to zero driving force to yield values of $(4.8 \pm 0.3) \times 10^4$ s^{-1}, $(2.5 \pm 0.2) \times 10^5$ s^{-1}, and $(3.3 \pm 0.3) \times 10^4$ s^{-1} for $k°_{3+/2+}$, $k°_{2+/1+}$, and $k°_{1+/0}$, respectively. For large values of η, these Tafel plots are curved for all three redox reactions, and while those corresponding to metal-based electron transfer are asymmetric with respect to η, those corresponding to ligand-based reactions are symmetric. Temperature-resolved measurements of k reveal that the electrochemical activation enthalpy, $\Delta H^{\ddagger}$, decreases from 43.1 ± 2.8 kJ mol^{-1} for the 3+/2+ reaction to 25.8 ± 1.9 kJ mol^{-1} for the 1+/0 process. Probing the temperature dependence of the formal potential gives the reaction entropy, $\Delta S_{rc}°$. The reaction entropy depends on the state of charge of the monolayer with values of 212 ± 18, 119 ± 9, and 41 ± 5 J mol^{-1} K^{-1} being observed for the 3+/2+, 2+/1+, and 1+/0, redox transformations, respectively. The electronic transmission coefficient, κ_{el}, describing the probability of electron transfer once the nuclear transition state has been reached, is considerably less than unity for all three redox processes. However, κ_{el} is larger for the bipyridyl-based reductions, $(2.4 \pm 0.9) \times 10^{-5}$, than for the metal-based reaction, $(1.5 \pm 0.7) \times 10^{-6}$. This large difference in electronic transmission coefficients may be a consequence of the redox potentials of the bridging ligand and the remote redox sites being comparable, so that the electronic states of the bridging ligand contribute to the electron tunneling pathway.

Introduction

Exploring the degree and mechanism of electronic interaction between remote redox centers and an underlying electrode surface on which they are adsorbed has been the subject of many experimental and theoretical investigations.[1] Particular attention has been focused on self-assembled ferrocene−alkanethiol systems in which a redox inactive alkane chain acts as a bridging ligand between the remote redox centers and the electrode surface.[2] The highly ordered structure of these self-assembled monolayers makes them useful model systems for probing fundamental issues such as the dependence of the heterogeneous electron transfer rate on the reaction free energy,[1c,d,3] the electron transfer distance,[4] and the molecular structure of the interface[5] and for investigating the role of ionic interactions in dictating electrochemical responses.[6]

However, redox active components can also be used as bridging ligands, offering the possibility of significant virtual coupling (superexchange) if the redox potentials of the bridge and remote redox centers are similar.[7] Electron transfer via superexchange may be the dominant mechanism if the LUMO of the bridge is close in energy to the donor and acceptor. This pathway predominates because the closeness of the bridge and redox center energies acts to reduce the activation barrier to electron tunneling. However, for long-range electron transfer reactions where the redox potentials of bridge and reacting species are very different, through-space electron transfer pathways may become important.

[⊗] Abstract published in *Advance ACS Abstracts,* April 15, 1996.

(1) (a) Dubois, L. H.; Nuzzo, R. G. *Ann. Rev. Phys. Chem.* **1992**, *43*, 437. (b) Richardson, J. N.; Rowe, G. K.; Carter, M. T.; Tender, L. M.; Curtin, L. S.; Peck, S. P.; Murray, R. W. *Electrochim. Acta* **1995**, *40*, 1331. (c) Chidsey, C. E. D.; Loiacono, D. N. *Langmuir* **1990**, *6*, 682. (d) Finklea, H. O.; Hanshew, D. D. *J. Am. Chem. Soc.* **1992**, *114*, 3173. (e) Forster, R. J.; Faulkner, L. R. *J. Am. Chem. Soc.* **1994**, *116*, 5453. (f) Chidsey, C. E. D.; Bertozzi, C. R.; Putvinski, T. M.; Mujsce, A. M. *J. Am. Chem. Soc.* **1990**, *112*, 4301. (g) Li, T.-T.; Weaver, M. J. *J. Am. Chem. Soc.* **1984**, *106*, 6107.

(2) (a) Chidsey, C. E. D. *Science* **1991**, *251*, 919. (b) Goss, C. A.; Miller, C. J.; Majda, M. *J. Phys. Chem.* **1988**, *92*, 1937. (c) Rubinstein, I.; Steinberg, S.; Tor, Y.; Shanzer, A. *Nature* **1988**, *332*, 426. (d) Weber, K.; Creager, S. E. *Anal. Chem.* **1994**, *66*, 3164. (e) Donohue, J. J.; Buttry, D. A. *Langmuir* **1988**, *4*, 671. (f) Collard, D. M.; Fox, M. A. *Langmuir* **1991**, *7*, 1192. (g) Lee, K. A. B. *Langmuir* **1990**, *6*, 709. (h) Uosaki, K.; Sato, Y.; Kita, H. *Langmuir* **1991**, *7*, 1510.

(3) Tender, L.; Carter, M. T.; Murray, R. W. *Anal. Chem.* **1994**, *66*, 3173.

(4) (a) Murray, R. W. *Molecular Design of Electrode Surfaces*; Wiley-Interscience: New York, 1992. (b) Becka, A. M.; Miller, C. J. *J. Phys. Chem.* **1993**, *97*, 6233.

(5) (a) Finklea, H. O.; Snider, D. A.; Fedik, J. *Langmuir* **1990**, *6*, 371. (b) Ulman, A. *An Introduction to Ultra-thin Organic Film From Langmuir-Blodgett to Self-Assembly*; Academic Press: San Diego, 1991.

(6) (a) De Long, H. C.; Donohue, J. J.; Buttry, D. A. *Langmuir* **1991**, *7*, 2196. (b) Redepenning, J.; Tunison, H. M.; Finklea, H. O. *Langmuir* **1993**, *9*, 1404. (c) De Long, H.; Buttry, D. A. *Langmuir* **1992**, *8*, 2491. (d) Nordyke, L. L.; Buttry, D. A. *Langmuir* **1991**, *7*, 380. (e) Rowe, G. K.; Creager, S. E. *Langmuir* **1991**, *7*, 2307.

(7) (a) Newton, M. D. *Chem. Rev.* **1991**, *91*, 767. (b) Miller, J. R.; Beitz, J. V. *J. Chem. Phys.* **1981**, *74*, 6746. (c) Closs, J. L.; Miller, J. R. *Science* **1988**, *240*, 440. (d) Onuchic, J. N.; Beratan, D. N. *J. Am. Chem. Soc.* **1987**, *109*, 6771. (e) Beratan, D. N. *J. Am. Chem. Soc.* **1986**, *108*, 4321.

S0020-1669(95)01343-7 CCC: $12.00

Scheme 1

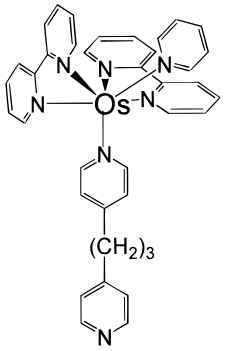

This contribution reports an investigation into these effects for osmium-containing monolayers that are spontaneously adsorbed onto platinum microelectrodes. These immobilized monolayers have been formed by including a 4,4′-bipyridyl type bridging ligand within the coordination shell of the osmium complex.[1e,8] One pyridine is bound to the central metal while the other is available for adsorption onto clean platinum surfaces. The monolayer of interest here is $[Os(bpy)_2py(p3p)]^{2+}$ (Scheme 1), where bpy is 2,2′-bipyridyl, py is pyridine, and p3p is 4,4′-trimethylenedipyridine. For simplicity, it is labeled here as [py(p3p)]. Abrûna and co-workers have probed the electron transfer characteristics and solvent dependence of the formal potential, for redox active self-assembling monolayers based on similar osmium complexes.[9] We have also probed the kinetics of heterogeneous electron transfer associated with the $Os^{2+/3+}$ redox reaction within a family of these monolayers using high-speed chronoamperometry.[1e,8]

Here, we focus on how the proximity of the bridge energy levels to the formal potential of the adsorbed redox centers affects the electron tunneling pathway. These adsorbed monolayers are excellent model systems for probing this issue since they undergo both metal- and bypyridyl-based electron transfer reactions. The redox potentials for these metal- and ligand-based processes are separated by at least 2.0 V, and while the redox potential of the metal-based oxidation is far from that of the bridging ligand, the bipyridyl-based reductions are within 0.3 V of the half-wave potential for the reduction of the uncomplexed bridging ligand.

The kinetic aspects of heterogeneous electron transfer to these three redox couples have been studied via chronoamperometry conducted on a microsecond time scale. These responses are remarkably well-behaved over a wide range of time scales, temperatures, and potentials allowing molecular bridge effects, in particular mediating electronic states of the bridging ligand (superexchange), on distant charge tunneling to be investigated.

The free energies of activation are different for each of the three redox couples, emphasizing the importance of considering differences in reaction energetics when attempting to evaluate the degree of donor/acceptor electronic coupling from rate data. The electronic transmission coefficients, κ_{el}, describing the probability of electron transfer once the transition state has been reached, are all considerably less than unity suggesting a nonadiabatic reaction involving weak electronic interaction between the electronic manifolds on the two sides of the interface. However, the values of κ_{el} observed for the ligand-based electron transfer reactions are more than an order of magnitude larger than those observed for the metal-based reaction. These investigations suggest that two-state models that consider just the donor and acceptor may not account for important factors that influence the rate of heterogeneous electron transfer across metal/monolayer interfaces.

Experimental Section

Materials. The surface active complex, $[Os(bpy)_2py(p3p)]^{2+}$, was prepared from $[Os(bpy)_2Cl(p3p)]^{2+}$ which was synthesized as described previously:[1e] 74 mg (0.1 mmol) of $[Os(bpy)_2Cl(p3p)]^{2+}$ was placed in 40 cm^3 of methanol and refluxed for 10 min to ensure complete dissolution. A solution of 20 mg (0.25 mmol) of pyridine dissolved in 5 cm^3 of methanol and 50 cm^3 of water were added, and the solution was refluxed for 15 h. After approximately 10−12 h the color of the solution changed from red-brown to dark green. The progress of the reaction was monitored using HPLC and cyclic voltammetry. After the reaction was complete, the volume was reduced to 5 cm^3 by rotary evaporation. Ammonium hexafluorophosphate (95+%, Aldrich) was then added, and the dark green product was collected by filtration and washed with diethyl ether. The product was recrystallized from aqueous methanol to give dark green-black crystals, yield 68 mg, 87%. The complex was characterized using IR, UV−vis, NMR, and cyclic voltammetry.

Apparatus. Electrochemical cells were of conventional design and were thermostated within ±0.2 °C using a Julabo F10-HC refrigerated circulating bath. All potentials are quoted with respect to a BAS Ag/AgCl gel-filled reference electrode, the potential of which was 35 mV more positive than that of the saturated calomel electrode (SCE). Cyclic voltammetry was performed using an EG&G Model 273 potentiostat/galvanostat and a conventional three-electrode cell. All solutions were degassed using nitrogen, and a blanket of nitrogen was maintained over the solution during all experiments.

In high-speed chronoamperometry,[10] a custom built function generator−potentiostat, with a rise time of less than 10 ns, was used to apply potential steps of variable pulse width and amplitude directly to a two-electrode cell. A Pt foil and an Ag/AgCl reference electrode were combined to form a counter electrode. The foil lowered the resistance and provided a high-frequency path.

Microelectrodes were fabricated from platinum microwires (Goodfellow Metals Ltd.) of radii between 1 and 25 μm by sealing them in soft glass using a procedure described previously.[10a] Microdisk electrodes were exposed by removing excess glass using 600 grit emery paper followed by successive polishing with 12.5, 5, 1, 0.3, and 0.05 μm alumina. The polishing material was removed between changes of particle size by sonicating the electrodes in deionized water for at least 5 min. The polished electrodes were electrochemically cleaned by cycling in 0.1 M $HClO_4$ between potential limits chosen to first oxidize and then to reduce the surface of the platinum electrode. Excessive cycling was avoided to minimize the extent of surface roughening. Finally, the electrode was cycled between −0.300 and 0.900 V in aqueous 0.1 M $NaClO_4$ until hydrogen desorption was complete.

The real or microscopic surface area of the electrodes was found by calculating the charge under the oxide or hydrogen adsorption−desorption peaks.[11] Typically, the surface roughness factor was between 1.3 and 1.6. Obtaining the real, as opposed to the projected or geometric, surface area of the electrodes is important if the area occupied per molecule is to be accurately measured.

The cell time constants, measured in blank electrolyte solution, were between 0.05 and 5 μs depending on the electrode radius and the supporting electrolyte concentration. The interfacial kinetics were measured only at times greater than about 5−10 times the cell time constant. This condition was satisfied by selecting a microelectrode of appropriate radius. The electrode radius is an important variable,

(8) (a) Forster, R. J.; Faulkner, L. R. *J. Am. Chem. Soc.* **1994**, *116*, 5444. (b) Forster, R. J.; Faulkner, L. R. *Anal. Chem.* **1995**, *67*, 1232. (c) Forster, R. J.; Faulkner, L. R. *Langmuir* **1995**, *11*, 1014. (d) Forster, R. J.; O'Kelly, J. P. *J. Phys. Chem.* **1996**, *100*, 3695.

(9) (a) Acevedo, D.; Abrûna, H. D. *J. Phys. Chem.* **1991**, *95*, 9590. (b) Acevedo, D.; Bretz, R. L.; Tirado, J. D.; Abrûna, H. D. *Langmuir* **1994**, *10*, 1300.

(10) (a) Xu, C. Ph.D. Thesis, University of Illinois at Urbana−Champaign, 1992. (b) Faulkner, L. R.; Walsh, M. R.; Xu, C. *Contemporary Electroanalytical Chemistry*; Plenum Press: New York, 1990.

(11) Trasatti, S.; Petrii, O. A. *J. Electroanal. Chem.* **1992**, *327*, 354.

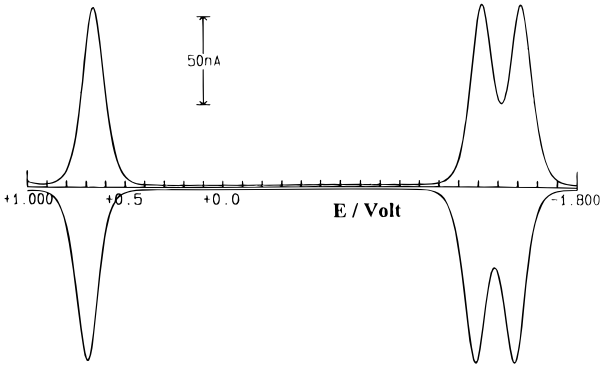

Figure 1. Cyclic voltammogram of a spontaneously adsorbed [py(p3p)] monolayer. The scan rate is 50 V/s, the surface coverage is 9.5×10^{-11} mol cm^{-2}. The supporting electrolyte is 0.1 M $TBABF_4$ in acetonitrile. The radius of the platinum microelectrode is 25 μm. The cathodic currents are up, and the anodic currents are down. The complex is in the $[py(p3p)]^{2+}$ form between +0.400 and −1.200 V. The initial potential was 1.000 V.

not only for ensuring fast double layer charging but also to ensure that the effects of uncompensated resistance on the measured rate constants are minimal.

Spontaneously adsorbed monolayers were formed *in situ* using a 100 μm solution of the metal complex in the electrolyte solution of interest. Unless otherwise stated, all electrochemical measurements were performed with this concentration of $[Os(bpy)_2py(p3p)]^{2+}$ in solution. A low concentration of the surface active complex in solution improved the stability of the monolayers when exposed to organic solvents, yet minimized the diffusional contribution to the overall current in chronoamperometry or cyclic voltammetry.

A nonisothermal cell, where the reference electrode was isolated from the main compartment by a salt bridge and held at room temperature, was used for the temperature-resolved experiments. The nonisothermal salt bridge contained saturated KCl since it has a low resistance and the salt remains soluble at the lowest temperature employed (−5 °C). The high electrolyte concentration and the design of the bridge minimize any systematic error in the reported temperature effects on $E^{\circ\prime}$ due to changes in the liquid junction potential with temperature.[12]

Results and Discussion

General Electrochemical Properties. Figure 1 shows a representative cyclic voltammogram for a spontaneously adsorbed [py(p3p)] monolayer, where the supporting electrolyte is 0.1 M tetrabutylammonium tetrafluoroborate ($TBABF_4$) in acetonitrile. The formal potentials, $E^{\circ\prime}$, are 0.680, −1.340, and −1.540 V and correspond to the metal-based $Os^{2+/3+}$ redox reaction and successive ligand-based reductions, respectively.[13] The corresponding formal potentials for a solution-phase model compound, $[Os(bpy)_3]^{2+}$, are identical within 30 mV. This experimental voltammetric response is consistent in all respects with that expected for an electrochemically reversible reaction involving a surface-confined species.[14] For example, the peak shapes are independent of scan rate, ν, at least over the range 1−50 V/s, and the peak height scales linearly with the scan rate unlike the $\nu^{1/2}$ dependence expected for a freely diffusing species. Therefore, it appears that the osmium complex adsorbs onto the surface of a platinum microelectrode to give an electroactive film. Brown and Anson, as well as Laviron, have demonstrated that the full width at half-maximum (fwhm) is sensitive to the degree of interaction between the adsorbates.[14] As the potential is scanned, the reduced (R) and oxidized (O) forms of the redox couple coexist near $E^{\circ\prime}$. Where there are no lateral interactions between surface-confined redox centers, or where the interactions between O and O, R and R, and O and R are large but similar to one another, a fwhm of 90.6 mV is expected for a reaction involving the transfer of a single electron. Therefore, while the overall electrochemical response of these monolayers is close to ideal, our experimental observation of a fwhm of between 95 and 110 mV does not allow us to reach a definite conclusion as to the degree of lateral interactions in these assemblies.

The peak height and peak area of the wave centered at 0.680 V do not change by more than 15% when cycled repeatedly over a 5 h period at temperatures up to 40 °C, indicating that the monolayers are thermally stable. In contrast to the behavior observed for the metal-based redox reaction, repeated cycling at slow scan rates causes the waves corresponding to the ligand-based reduction reactions to become increasingly less well-defined and causes the total charge to decrease. Moreover, $E^{\circ\prime}_{2+/3+}$ shifts in a positive potential direction. These observations suggest that heterogeneous electron transfer to give the neutral monolayer is followed by a chemical reaction. The half-life of this following chemical reaction depends strongly on the purity of the solvent, particularly its water content, but is on the order of 700 ms in dry acetonitrile. Therefore, to out run this following chemical reaction only scan rates greater than 1 V/s were used to characterize the bpy-based reductions.

The faradaic charge associated with converting the monolayer from the 2+ to the 3+ oxidation states has been estimated from under the wave centered at 0.680 V. This charge, together with the real surface area of the electrode, has been used to calculate the surface coverage, or the number of moles of $[Os(bpy)_2py(p3p)]^{2+}$ per square centimeter. The limiting surface coverage, Γ, was $(9.5 \pm 0.8) \times 10^{-11}$ mol cm^{-2}, corresponding to an area occupied per molecule of 175 ± 17 Å^2. When the additional contributions to the molecular volume are considered, e.g., a solvent shell or a counterion, this area of occupation is consistent with that expected for a close packed monolayer in which the radius of the metal complex (≈6.7 Å)[15] rather than the length of the bridging ligand dictates the surface coverage. This area of occupation is smaller than that found for adsorbed $[Os(bpy)_2Cl(p3p)]^+$ complexes[1e] (240 Å^2) but is indistinguishable from that found for adsorbed $[Os(bpy)_2(p3p)_2]^{2+}$ complexes.[8d]

The effect of the applied potential on the redox composition of the monolayer has been probed using chronocoulometry.[1e,16,17] Plots of ln([Ox][Red]) vs potential for the metal-based oxidation and ligand-based reduction reactions were all linear for absolute overpotentials η ($\equiv$ E − E$^{\circ\prime}$) less than 0.070 V. The slopes observed for the $Os^{3+/2+}$ redox reaction and the two ligand-based reduction are 55 ± 3, 51 ± 5, and 50 ± 6 mV/decade, respectively. These slopes are indistinguishable from those predicted for one-electron transfer reactions by the Nerst equation,[17] confirming that the thermodynamic aspects of electron transfer at these metal/monolayer interfaces are nearly ideal under the experimental conditions employed.

(12) Yee, E. L.; Cave, R. J.; Guyer, K. L.; Tyma, P. D.; Weaver, M. J. *J. Am. Chem. Soc.* **1979**, *101*, 1131.
(13) (a) Griffith, W. P. In *Comprehensive Coordination Chemistry*; Wilkinson, G., Ed.; Pergamon: Oxford, England, 1987; Vol. 4, Chapter 46. (b) Sullivan, B. P.; Conrad, D.; Meyer, T. J. *Inorg. Chem.* **1985**, *24*, 3640. (c) Tokel-Takvoryan, N. E.; Hemmingway, R. W.; Bard, A. J. *J. Am. Chem. Soc.* **1973**, *95*, 6582.
(14) (a) Laviron, E. *J. Electroanal. Chem.* **1974**, *52*, 395. (b) Brown, A. P.; Anson, F. C. *Anal. Chem.* **1977**, *49*, 1589.
(15) (a) Goodwin, H. A.; Kepert, D. L.; Patrick, J. M.; Skelton, B. W.; White, A. H. *Aust. J. Chem.* **1984**, *37*, 1817. (b) Ferguson, J. E.; Love, J. L.; Robinson, W. T. *Inorg. Chem.* **1972**, *11*, 1662. (c) Rillema, D. P.; Jones, D. S.; Levy, H. A. *J. Chem. Soc., Chem. Commun.* **1979**, 849.
(16) (a) Forster, R. J. *Langmuir* **1995**, *11*, 2247. (b) Forster, R. J.; Vos, J. G. *Langmuir* **1994**, *10*, 4330.
(17) Bard, A. J.; Faulkner, L. R. *Electrochemical Methods: Fundamentals and Applications*; Wiley: New York, 1980.

For supporting electrolyte concentrations above 0.1 M, the peak heights and shapes observed in cyclic voltammetry are independent of the electrolyte concentration. Below this electrolyte concentration, distortions in the voltammetric response are observed, particularly at high scan rates. These deviations from ideality are consistent with *iR* drop effects due to the relatively low conductivity of the electrolyte solution.[17] Significantly, the formal potentials of all three redox processes investigated are constant within 25 mV as the supporting electrolyte concentration is varied from 0.1 to 1.0 M. That $E^{\circ\prime}$ is independent of the supporting electrolyte concentrations, apart from liquid junction potential effects, suggests either that the same numbers of ions are paired with the oxidized and reduced forms of each of the redox couples[18] or that significant ion pairing does not occur where $TBABF_4$ is the supporting electrolyte.

Interfacial Capacitance. Probing the double layer capacitance C_{dl} gives an insight into the change in interfacial charge distribution that accompanies monolayer formation, the relative perfection of the monolayer, and perhaps its thickness.[19] Here, small amplitude potential step chronoamperometry has been used to measure the interfacial capacitance as the electrolyte concentration was systematically varied. The pulse amplitude ΔE was 25 mV, which is sufficiently small to allow the measured capacitance to be regarded as an approximate differential capacitance.[17] Stepping the potential in a region where the redox composition did not change, i.e., far from $E^{\circ\prime}$, gave only single exponential current decays due to double layer charging. When the potential was stepped in a region close to $E^{\circ\prime}$, two time-resolved first order decays were observed that correspond to double layer charging and the faradaic reaction, respectively (vide infra). These data can be used to obtain the resistance, *R*, and the total interfacial capacitance, C_T, according to the following relation.[20]

$$i_c(t) = (\Delta E/R)\exp(-t/RC_T) \quad (1)$$

For the monolayer-coated interfaces considered here, the reciprocal of the total interfacial capacitance can be represented by the sum of the reciprocal capacitances of the film, C_{film}, and the diffuse layer, C_{dif}[19a−d]

$$C_T^{-1} = C_{film}^{-1} + C_{dif}^{-1} \quad (2)$$

$$C_{film} = \epsilon_0\epsilon_{film}/d \quad (3)$$

$$C_{dif} = \epsilon_0\epsilon_{SOLN}\kappa\cosh[ze(\phi_{PET} - \phi_{SOLN})/2k_BT] \quad (4)$$

where ϵ_0 is the permittivity of free space, ϵ_{film} and ϵ_{SOLN} are the film and solution dielectric constants, respectively, *d* is the monolayer thickness, *z* is the charge number of the electrolyte ion, *e* is the absolute electronic charge, k_B is the Boltzmann constant, *T* is the absolute temperature, and ϕ_{PET} and ϕ_{SOLN} are the potentials at the plane of electron transfer and in the bulk solution, respectively. The quantity κ is given by $(2n^\circ z^2e^2/(\epsilon_{SOLN}\epsilon_0k_BT))^{1/2}$, where n° is the number concentration of the ions in solution.[17]

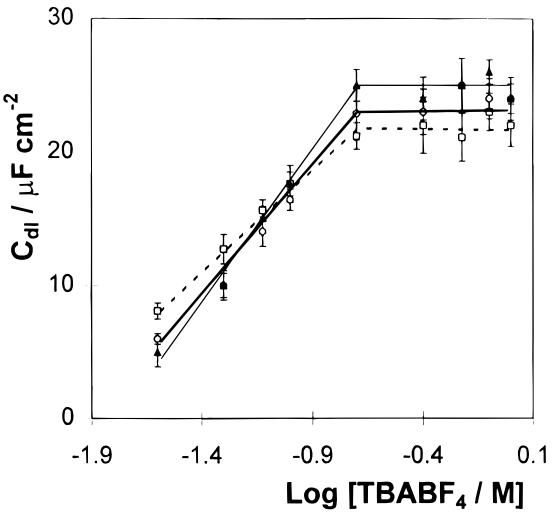

Figure 2. Dependence of the total interfacial capacitance for a spontaneously adsorbed [py(p3p)] monolayer on the logarithm of the supporting electrolyte concentration. From top to bottom, on the right-hand side, the capacitances were determined using a small amplitude potential step centered on 0.000, −1.500, and −1.800 V, respectively.

In the absence of specific adsorption of the electrolyte ions, only the diffuse layer capacitance is considered to depend on the potential or the concentration of supporting electrolyte. Therefore, the relative importance of that component may be probed by systematically varying the supporting electrolyte concentration and measuring the total capacitance. Figure 2 shows the approximate differential capacitance, determined at potentials of 0.000, −1.500, and −1.800 V, as a function of the logarithm of the supporting electrolyte concentration. The charge on the monolayer at these potentials is 2+, 1+, and 0, respectively. Figure 2 shows that at each of the three potentials investigated, the double layer capacitance increases approximately linearly with increasing logarithm of the electrolyte concentration for $TBABF_4$ concentrations less than about 0.2 M. This sensitivity indicates that the diffuse layer capacitance contributes to the total interfacial capacitance over this concentration range. Significantly, the slopes of these plots at low electrolyte concentration and the limiting value of C_T at high electrolyte concentration are largely independent of the monolayer's state of charge. These observations suggest that the composition of the medium at the electrode/monolayer interface does not depend on the applied potential, indicating that the monolayer structure does not change dramatically over the potential range of 0.000 to −1.800 V.

Figure 2 shows that the limiting capacitances at high electrolyte concentrations are at least 22−25 μF cm^{-2}. These data do not allow us to reach a conclusion as to whether this limiting capacitance represents the film capacitance or the capacitance of the charges held at the outer Helmholtz plane after the double layer sets up inside the monolayer. However, a capacitance of 22−25 μF cm^{-2} is considerably larger than that associated with a solvent free monolayer[19f] suggesting that the films considered here are solvated, at least at high concentrations of supporting electrolyte.

Chronoamperometry. For an ideal electrochemical reaction involving a surface bound species, the faradaic current following a potential step that changes the redox composition of the monolayer exhibits a single exponential decay in time

(18) (a) Creager, S. E.; Rowe, G. K. *Anal. Chim. Acta* **1991**, *246*, 233. (b) Nagamura, T.; Sakai, K. *Chem. Phys. Lett.* **1987**, *141*, 553. (c) Nagamura, T.; Sakai, K. *J. Chem. Soc., Faraday Trans.* **1988**, *84*, 3529.

(19) (a) Widrig, C. A.; Chung, C.; Porter, M. D. *J. Electroanal. Chem.* **1991**, *310*, 335. (b) Smith, C. P.; White, H. S. *Anal. Chem.* **1992**, *64*, 2398. (c) Creager, S. E.; Weber, K. *Langmuir* **1993**, *9*, 844. (d) Andreu, R.; Fawcett, W. R. *J. Phys. Chem.* **1994**, *98*, 12753. (e) Bryant, M. A.; Crooks, R. M. *Langmuir* **1993**, *9*, 385. (f) Porter, M. D.; Bright, T. B.; Allara, D. L.; Chidsey, C. E. D. *J. Am. Chem. Soc.* **1987**, *109*, 3559. (g) Nuzzo, R. G.; Allara, O. L. *J. Am. Chem. Soc.* **1983**, *105*, 4481.

(20) Wightman, R. M.; Wipf, D. O. *Electroanalytical Chemistry*; Bard, A. J., Ed.; Marcel Dekker: New York, 1989; Vol. 15.

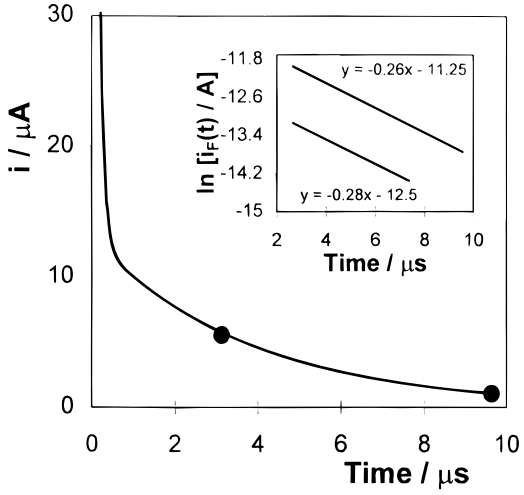

Figure 3. Current response for a 12.5 μm platinum microelectrode modified with a [py(p3p)] monolayer following a potential step where the overpotential η was -100 mV. The supporting electrolyte is 0.1 M $TBABF_4$ in acetonitrile. The inset shows ln $i_F(t)$ vs t plots for the Faradaic reaction for a 12.5 μm (top) and a 5 μm (bottom) radius platinum microelectrode.

according to:[1d,1e,2a,20]

$$i_F(t) = kQ \exp(-kt) \quad (5)$$

where k is the apparent rate constant for the overall reaction and Q is the total charge passed in the redox transformation.

Figure 3 illustrates a typical example of the chronoamperometric response observed for the $Os^{3+} + e^- \rightarrow Os^{2+}$ redox reaction of a [py(p3p)] monolayer, where the electrolyte is 0.1 M $TBABF_4$ in acetonitrile. In this experiment the potential was stepped from 1.000 to 0.580 V which corresponds to an overpotential η ($\equiv E - E^{\circ\prime}$) of -0.100 V. This figure shows that on a microsecond time domain two current decays can be separated. These responses, which arise from double layer charging and faradaic current flow, are time-resolved due to the much shorter time constant of double layer charging compared to that of the faradaic reaction. In these investigations, the electron transfer rate constant has been determined only when the time constant of double layer charging is at least 5 times shorter than the time constant of the faradaic reaction. This condition has been satisfied by carefully selecting the radius of the microelectrode.

While fast charging of the electrochemical double layer is undoubtedly important, the effects of ohmic losses must also be considered.[17] When faradaic and charging currents flow through a solution, they generate a potential that acts to weaken the applied potential by an amount iR, where i is the total current that flows through the solution. This ohmic drop can lead to severe distortions of experimental responses resulting in inaccurate measurements of the heterogeneous electron transfer rate. As illustrated in Figure 3, the faradaic currents that flow in these high-speed chronoamperometric experiments are typically in the low-microampere range even for 12.5 μm radius electrodes. Given that the cell resistance in this experiment is approximately 7000 Ω, the average iR drop is less than 35 mV for this system. However, the situation regarding ohmic effects is much more demanding when large overpotentials are employed because larger faradaic currents flow at short times. For example, the currents observed at a 12.5 μm modified electrode in a potential step experiment employing a 400 mV overpotential would be in the 100 μA range resulting in a massive ohmic loss. We have used three strategies to minimize the effects of uncompensated resistance in the large potential step experiments. First, we use a relatively high supporting electrolyte concentration (typically $\geq$0.2 M). Second, we use smaller electrodes to measure k at large overpotential. This approach is useful since the resistance increases with decreasing electrode radius but the current decreases as the square of the radius leading to reduced ohmic effects for smaller electrodes, e.g., the maximum ohmic loss observed at the highest overpotential employed is reduced from approximately 3000 mV at a 12.5 μm microelectrode to 240 mV at a 1 μm microelectrode. Third, and perhaps most importantly, we extract rate constants only from data obtained relatively later in the lifetime of the current decay transient, i.e., when the anticipated iR drop is less than 15 mV.

The linearity of the semilog plot shown in the inset of Figure 3 indicates that heterogeneous electron transfer associated with reduction of a $[py(p3p)]^{3+}$ monolayer is a first order process. For each of the three redox couples investigated, these responses are linear over approximately one and one-half lifetimes for the entire range of overpotentials employed, 50 mV $\leq |\eta| \leq$ 350 mV. Deviations from linearity would be expected if substantial ohmic drop effects were present. Uncompensated resistance causes the applied potential, and hence the apparent rate, to evolve with time. Therefore, iR drop would produce negative deviations in the observed current at short times.[17] That such nonidealities are not observed, at least for high concentrations of supporting electrolyte, is consistent with negligible ohmic losses. We have further probed the existence of ohmic effects by reducing the radius of the microelectrode. The inset in Figure 3 shows that the slope of the semilog plot obtained for a 5 μm platinum electrode modified with a spontaneously adsorbed [py(p3p)] monolayer is indistinguishable from that obtained at a 12.5 μm electrode. This observation is consistent with ohmic losses being negligible under the experimental conditions employed.

Further evidence supporting the predominance of a single rate constant at high concentrations of supporting electrolyte is obtained by examining the intercept of the semilog plot at zero time. As indicated by eq 5, the intercept for a single exponential decay is ln(kQ). Nernst plots of the redox composition as a function of potential (vide supra) confirm that an overpotential of -100 mV decreases the number of oxidized species within the monolayer to less than 3% of the total. Therefore, this potential step effectively causes complete reduction of the film, and the full surface coverage, Γ, can be calculated from the intercept of Figure 3 using the relation[14]

$$\Gamma = Q/(nFA) \quad (6)$$

where n is the number of electrons transferred, F is Faraday's constant, and A is the real or microscopic electrode area. This chronoamperometric determination of the charge passed can then be compared with the value determined using cyclic voltammetry to further test the ideality of the chronoamperometric response. We find that the charges passed in these two independent experiments agree within 10%. This agreement indicates that all of the surface-confined molecules are redox active on a microsecond time scale, i.e., relatively few, if any, sites are kinetically isolated.

Potential Dependence of *k*. Figure 4 illustrates Tafel plots of ln k vs overpotential, η, for the 3+/2+ and 2+/1+ redox reactions, where the supporting electrolyte is 0.2 M $TBABF_4$ in acetonitrile. This figure shows that, for overpotentials less than about 200 mV, ln k depends approximately linearly on η. The standard heterogeneous electron transfer rate constant, k°, has been determined by linearly extrapolating ln k to zero overpotential. The standard heterogeneous rate constant depends on the redox process being probed, and while a k° of

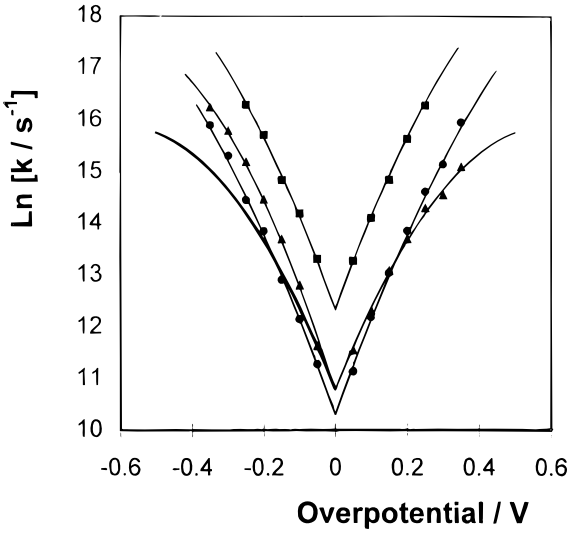

Figure 4. Tafel plots where ■, ▲, and ● denote experimental data for the 2+/1+, 3+/2+, and 1+/0 redox couples, respectively. The solid lines denote theoretical fits. The 2+/1+ and 1+/0 data are modeled using a through-bond tunneling approach in which the solvent reorganization energies equal 62 and 80 kJ mol^{-1}, respectively. The 3+/2+ data are modeled using a through-space tunneling approach in which the solvent reorganization energy is 48 kJ mol^{-1}. The heavy solid line indicates the behavior expected for metal-based heterogeneous electron transfer occurring via a through-bond tunneling mechanism. The supporting electrolyte is 0.2 M $TBABF_4$ in acetonitrile. The errors in the rate constants are approximately equal to the size of the symbols.

$(4.8 \pm 0.3) \times 10^4$ s^{-1} is observed for the metal-based 3+/2+ reaction, a significantly higher standard rate constant of $(2.5 \pm 0.2) \times 10^5$ s^{-1} is observed for the first ligand-based reduction. The origin of these differences is explored in greater detail later. This paper is not the first to measure the electron transfer kinetics of the redox couples within this type of polypyridyl complex. For example, Wightman and co-workers probed the heterogeneous electron transfer rate of the structurally related ruthenium tripyridyl complex dissolved in acetonitrile and observed rate constants of 2.5 and 3.4 cm s^{-1} for the 2+/1+ and 1+/0 couples, respectively.[21] The electrochemical properties of similar complexes adsorbed on an electrode surface have also been considered, e.g., Murray and Jernigan probed the rates of electron self-exchange reactions between Os(III) and Os(II) and between Os(II) and Os(I) sites within polymeric coatings.[22] The data reported here confirm the observation of these previous studies that electron transfer occurs very rapidly within systems of this type.

To probe the influence of counterion availability and double layer effects on heterogeneous electron transfer in these systems, we have measured $k°$ as the concentration of supporting electrolyte is systematically varied, and Table 1 contains the data. The intermonolayer precision in $k°$ is less than 10% suggesting that the monolayer structure is highly reproducible between different coatings. Table 1 reveals that $k°$ for the 3+/2+ and 2+/1+ couples increase by approximately 15% and 25%, respectively, as the concentration of the supporting electrolyte is increased from 0.1 to 1.0 M. This observation is consistent with the presence of a small ohmic loss in low concentrations of supporting electrolyte. The experimental cell resistance decreases from approximately 7000 Ω in 0.1 M $TBABF_4$ to approximately 4800 Ω in 1.0 M $TBABF_4$. This reduced cell resistance at high concentrations of supporting electrolyte decreases the maximum ohmic loss from approximately 35 to 25 mV, i.e., it increases the driving force for heterogeneous electron transfer by approximately 10 mV in 1.0 M $TBABF_4$ compared to the situation in 0.1 M $TBABF_4$. The variation in $k°$ shown in Table 1 is consistent with this slightly increased driving force at high concentrations of supporting electrolyte. On the basis of these data we conclude that diffusion/migration of charge-compensating counterions does not influence the measured heterogeneous electron transfer rate constant and that it is the dynamics of elementary electron transfer evens that are probed in high-speed chronoamperometry.

Table 1. Dependence of the Standard Heterogeneous Rate Constant, $k°$, on the Supporting Electrolyte Concentration for Metal- and Ligand-Based Electron Transfer Reactions within [py(p3p)] Monolayers[a]

$[TBABF_4]$, M	$10^{-4}k°_{3+/2+}$, s^{-1}	$10^{-5}k°_{2+/1+}$, s^{-1}	$10^{-4}k°_{1+/0}$, s^{-1}
0.10	4.4(0.3)	2.1(0.2)	3.0(0.2)
0.20	4.8(0.4)	2.2(0.2)	3.2(0.3)
0.50	4.9(0.3)	2.7(0.1)	3.3(0.2)
0.75	5.1(0.2)	2.6(0.2)	3.4(0.2)
1.00	5.2(0.2)	2.8(0.1)	3.3(0.3)

[a] Numbers in parentheses represent the standard deviations for at least three individual monolayers. Supporting electrolyte is tetrabutylammonium tetrafluoroborate ($TBABF_4$) in acetonitrile. All rate constants were determined at 298 K.

The dependence of ln k on η is clearly nonlinear at large overpotentials, and the slopes decrease in magnitude with increasing overpotential in both the anodic and cathodic directions. There are a number of possible explanations for the observed curvature, e.g., double layer effects caused by anion adsorption at the positive potentials used to probe the oxidation kinetics of the 2+ complex, the oxidation of trace water to form an oxide barrier, or structural imperfections within the monolayer. The possibility that the rate data presented here are affected by artifacts cannot be unequivocally ruled out. However, that the semilog current vs time plots remain linear at high overpotentials, and over a wide range of time scales, supporting electrolyte concentrations, and temperatures suggests that parasitic side reactions are negligible.

Simplified models based on the Marcus theory[3,23] that consider the effects of solvent reorganization have been developed to model heterogeneous electron transfer across electrode/monolayer interfaces.[1d,2a] Chidsey,[2a] as well as Finklea et al.,[1d] have independently assembled models describing the effects of electron tunneling on the electron transfer rates. For a through-bond tunneling mechanism, these models predict that Tafel plots will be symmetric with respect to overpotential. That symmetric Tafel plots are observed for both ligand-based reductions suggests that electron transfer to the bypyridyl ligands may occur via a through-bond tunneling pathway, perhaps mediated by electronic states within the bridging ligand. In contrast, Figure 4 shows that for the $Os^{2+/3+}$ couple larger cathodic than anodic heterogeneous electron transfer rate constants are observed for a given absolute value of the overpotential perhaps suggesting a through-space tunneling process.

We have used Finklea and Hanshew's model to estimate reorganization energies and hence free energies of activation $\Delta G^{\ddagger}$, for the metal- and ligand-based redox processes. This is an important objective because the heterogeneous electron transfer rate is considered to depend on a frequency factor and

(21) Wipf, D. O.; Kristensen, E. W.; Deakin, M. R.; Wightman, R. M. *Anal. Chem.* **1988**, *60*, 306.
(22) Jernigan, J. C.; Murray, R. W. *J. Am. Chem. Soc.* **1987**, *109*, 1738.
(23) (a) Marcus, R. A. *J. Chem. Phys.* **1956**, *24*, 966. (b) Marcus, R. A. *J. Chem. Phys.* **1965**, *43*, 679.

a Franck−Condon barrier and can be expressed as[24]

$$k = \tau_n \kappa_{el} \nu_n \exp(-\Delta G^{\ddagger}/RT) \quad (7)$$

where Γ_n is the nuclear tunneling factor, κ_{el} is the electronic transmission coefficient, and ν_n is the nuclear frequency factor.[25,26] We assume that the nuclear tunneling factor is unity and that it is temperature independent.[24] From eq 7, it is evident that the different standard heterogeneous electron transfer rate constants observed for the metal- and ligand-based redox reactions could be caused by changes in the free energy of activation or the preexponential factor. Since the free energy of activation, $\Delta G^{\ddagger}$, equal $\lambda/4$, where λ is the total reorganization energy associated with switching the oxidation state of the monolayer, an important objective is to experimentally measure λ.

In Finklea's model,[1d] the heterogeneous electron transfer rate constant for electron transfer without through-space tunneling is given by the integral over energy of the Fermi function of the metal, $n(\xi)$, and the distribution of energy levels for acceptor or donor states in the monolayer, $D(\xi)$, which is assumed to be Gaussian. To account for the effects of through-space tunneling, a rate parameter for electron tunneling at a given energy is added. Since these models predict Tafel plots that are symmetric with respect to overpotential for through-bond tunneling, while those for through-space are predicted to be asymmetric, this approach can provide an insight into the mechanism of electron transfer in these systems.

To fit either the through-space or through-bond tunneling models to the experimental data shown in Figure 4, estimates are required for the average barrier height for direct elastic tunneling through a trapezoidal energy barrier, E_B, the total reorganization energy associated with switching the redox state of the monolayer, λ, and the preintegral factor.

The average barrier height for electron tunneling at $[Os(bpy)_2Cl(pNp)]^+$ monolayers, where pNp is 4,4′-dipyridyl, 1,2-bis(4-pyridyl)ethane, or 4,4′-trimethylenedipyridine, has previously been estimated from the distance dependence of $k°$.[1e] Given that the same bridging ligand is used here, we employ the same value of the average barrier height to electron tunneling, 200 kJ mol^{-1}, in the present analysis. The total reorganization energy, λ, dictates the degree of curvature in the Tafel plots. Therefore, λ was chosen so that there was satisfactory agreement between shapes of the theoretical Tafel plots and the experimental data. Finally, the preintegral factor was adjusted to give the experimental value of $k°$. In the Finklea model, the tunneling parameter, β, describing the exponential decrease in the electron tunneling probability with increasing distance, is considered to depend on potential. However, in agreement with reports on other monolayer systems,[8a,27] we find that the experimentally observed potential dependence of k can be accurately modeled using a single reorganization energy for both anodic and cathodic branches, if β is held constant throughout the integration.

Figure 4 shows that satisfactory agreement between Finklea and Hanshew's through-space tunneling model and the experimental data for the $Os^{2+/3+}$ couple is obtained when λ is 48 kJ mol^{-1}. An alternative explanation of the asymmetry observed in the Tafel plot for the 2+/3+ redox couple is that the reorganization energy for monolayer oxidation is smaller than that for reduction. However, the through-space tunneling mechanism is attractive since it accurately models both the anodic and cathodic branches using a single value of the reorganization energy. A through-space tunneling mechanism for the metal-based electron transfer reaction indicates that there is insufficient overlap between the delocalized metallic states of the electrode and the spatially localized orbitals of the redox center to allow direct electron transfer. However, while the symmetrical response observed for the first ligand-based reduction reaction cannot be modeled using the through-space tunneling approach used for the metal-based reaction, it can be simply modeled using a through-bond tunneling model. Satisfactory agreement between the experimental data and the theoretical through-bond estimates is observed for the 2+/1+ and 1+/0 couples when the reorganization energies are 62 and 80 kJ mol^{-1}, respectively. It appears unlikely that the bipyridyl-based redox reactions proceed via a through-bond mechanism without involving the aromatic p3p bridging ligand. It is perhaps useful to consider the effect that the large difference is formal potentials for the metal- and ligand-based reactions may have on the electron tunneling pathway. For the present system, the redox potentials of the $Os^{2+/3+}$ couple and the p3p bridging ligand are separated by at least 2.5 V, while the redox potentials of the p3p and bipyridyl ligands are within 0.3 V of one another. Therefore, since the energies of the bridge LUMO and the bipyridyl ligands are close in energy, it is possible that a through-bond superexchange mechanism involving mediating electronic states within the bridging ligand represents the electron tunneling pathway for the bipyridyl-based reactions.

The Marcus approach can provide a theoretical estimate of the reorganization energy.[23a,b] In the Marcus model, λ is considered to be the sum of an inner sphere and outer sphere component. The inner sphere component describes the distortion of bond angles and lengths accompanying electron transfer, while the outer sphere component reflects solvent reorganization effects. The outer sphere solvent reorganization energy λ_{OS} is given by

$$\lambda_{OS} = (\Delta e^2/2)(r^{-1} - R_e^{-1})(\epsilon_{op}^{-1} - \epsilon_s^{-1}) \quad (8)$$

where e is the absolute electronic charge, r is the radius of the metal complex (6.7 Å), R_e is the reactant−image distance, ϵ_{op} is the optical dielectric constant of acetonitrile and is taken as being equal to the square of the refractive index (1.795), and ϵ_{SOLN} is the static dielectric constant (37.5). As discussed previously,[1e] we have neglected imaging effects, i.e., $R_e \rightarrow \infty$, in calculating the theoretical solvent reorganization energy. Equation 8 yields a solvent reorganization energy of 56 kJ mol^{-1}, which agrees rather well with the values of 48 and 62 kJ mol^{-1} obtained from fitting the data illustrated in Figure 4 for the $[py(p3p)]^{3+/1+}$ couples, respectively.

Solid state crystallographic data indicate that changing the oxidation state of the metal center within osmium and ruthenium polypyridyl complexes does not significantly change either the bond lengths or angles.[15] Therefore, the inner sphere reorganization energy is negligible, at least for the 3+/2+ couple in the solid state. That our experimental reorganization energies are within 20% of that predicted for outer sphere solvent reorganization suggests that the activation energy barrier to heterogeneous electron transfer for the 3+/2+ and 2+/1+ couples is dominated by solvent reorganization. In contrast, while the experimental data for the 1+/0 couple are consistent

(24) (a) Weaver, M. J. *Chem. Rev.* **1992**, *92*, 463. (b) Bagchi, G. *Annu. Rev. Phys. Chem.* **1989**, *40*, 115. (c) Sutin, N. *Acc. Chem. Res.* **1982**, *15*, 275.
(25) (a) Sutin, N. *Prog. Inorg. Chem.* **1983**, *30*, 441. (b) Hupp, J. T.; Weaver, M. J. *J. Electroanal. Chem.* **1983**, *145*, 43. (c) Fawcett, W. R.; Foss, C. A. *J. Electroanal. Chem.* **1989**, *270*, 103.
(26) Sutin, N.; Brunschwig, B. S. *ACS Symp. Ser.* **1982**, *198*, 105.
(27) (a) Becka, A. M.; Miller, C. J. *J. Phys. Chem.* **1992**, *96*, 2657. (b) Xu, J.; Li, H.-L.; Zhang, Y. *J. Phys. Chem.* **1993**, *97*, 11497. (c) Kornyshev, A. A.; Kuznetsov, A. M.; Ulstrup, J. *J. Phys. Chem.* **1994**, *98*, 3832.

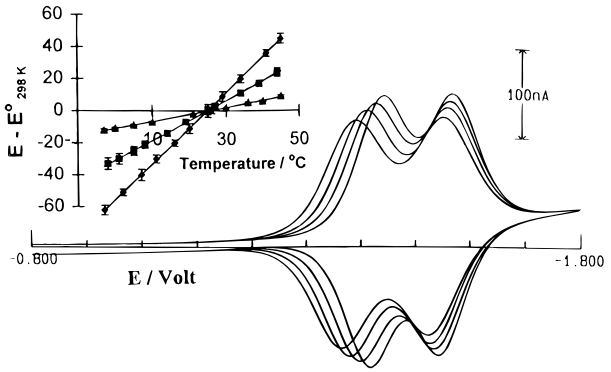

Figure 5. Effect of temperature on the cyclic voltammetry of a [py(p3p)] monolayer in contact with 0.5 M $TBABF_4$ in acetonitrile as supporting electrolyte. The temperatures are, from right to left, −5, 10, 25, and 40 °C. The scan rate is 50 V/s. Both anodic and cathodic branches shift equally with changes in temperature. The inset shows the temperature dependence of the formal potentials normalized with respect to their formal potentials measured at 298 K. From top to bottom on the right-hand side the data represent the 3+/2+, 2+/1+, and 1+/0 couples, respectively.

with a through-bond tunneling mechanism, the experimental reorganization energy (80 kJ mol^{-1}) is significantly larger than that predicted by eq 7 for solvent reorganization alone. This observation would be consistent with the second ligand-based reduction reaction changing the OS−bpy bond lengths or angles or perhaps triggering a structural change within the adsorbed monolayer that acts as an "inner sphere" barrier to heterogeneous electron transfer.

We note that the electron transfer dynamics can only be probed over a restricted range of overpotentials because of the rapid nature of the process and the interference from double layer charging effects at times below 100 ns. To eliminate the inherent inaccuray of fitting Tafel plots over a limited potential range to estimate λ, temperature-resolved measurements of the formal potential and heterogeneous electron transfer rate have been performed. These measurements independently measure the electrochemical activation entropy and enthalpy, respectively.

Reaction Entropies. The reaction entropy, $\Delta S_{rc}°$, quantifies the difference in entropy between the reduced and oxidized forms of the redox couple. If $\Delta S_{rc}°$ were very different for the metal- and ligand-based electron transfer reactions, then it could explain the differences in the free energy of activation for metal- and ligand-based reactions suggested by Figure 4. Moreover, since several different oxidation states can be accessed, the monolayer system reported here provides an important opportunity to probe the functional dependence of the reaction entropy on the state of charge of the monolayer.[28]

The reaction entropy has been determined using a nonisothermal cell by measuring the temperature dependence of the formal potentials for both metal- and bpy-based electron transfer reactions. As discussed by Weaver and co-workers, the temperature dependence of the formal potential can be expressed as[28,29]

$$\Delta S_{rc}° = F(\partial E°'/\partial T) \quad (9)$$

Figure 5 shows representative temperature-dependent cyclic voltammograms for the two ligand-based reductions. For the situations investigated, all three formal potentials shift in a positive potential direction with increasing temperature. This observation indicates positive reaction entropies and a higher degree of local ordering in the oxidized, than in the reduced, state. As shown in the inset of Figure 5, plots of $E°'$ vs T are linear over the temperature range −5 to 40 °C, and reaction entropies have been calculated from the slopes according to eq 9. Experimentally, the magnitude of $\Delta S_{rc}°$ depends on the redox process being investigated, with values of 212 ± 18, 119 ± 9, and 41 ± 5 J mol^{-1} K^{-1} being observed for the 2+/3+, 1+/2+, and 0/1+ redox couples, respectively.

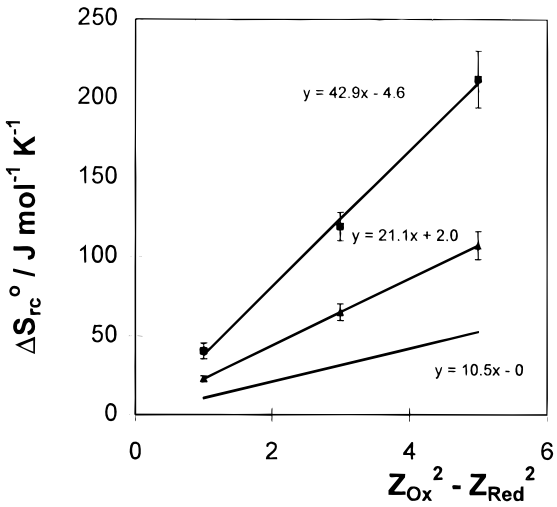

Figure 6. Reaction entropies for [py(p3p)] monolayers (top), solution phase [Os(bpy)$_3$] (middle), and the predictions of the Born model (bottom) vs the difference in the square of the charge numbers for the oxidized and reduced states. The supporting electrolyte is 0.1 M $TBABF_4$ in acetonitrile.

The dielectric continuum theory can provide an estimate of the reaction entropy via the Born equation,[30]

$$\Delta S_{re}°(\text{Born}) = -N_A \Delta e^2 (\partial \epsilon_s/\partial T)[(z_R + 1)^2 - z_R^2]/(2r\epsilon_s^2) \quad (10)$$

where N_A is Avogadro's number, e is the electronic charge, ϵ_s is the static dielectric constant, Z_R is the charge on the reduced form of the redox couple, and r is the radius of the complex. Figure 6 illustrates the dependence of the experimental reaction entropies and the estimates provided by eq 10 on ($Z_{Ox}^2 - Z_{Red}^2$). This figure shows that the experimental reaction entropy is indeed quadratically dependent on the ionic charge for this monolayer system. However, eq 10 predicts reaction entropies that are significantly smaller, and less sensitive to the ionic charge, than those experimentally observed. To investigate whether these observations are a consequence of the molecules being confined within a dense monolayer, the reaction entropies for the solution phase analog, [Os(bpy)$_3$](PF$_6$)$_2$, have also been measured, and the data are included in Figure 6. As has been observed previously by Hupp and Weaver for solution-phase $[Ru(bpy)_3]^{n+}$ in acetonitrile,[28] the experimental reaction entropies for dissolved polypyridyl complexes tend to be larger than those predicted by eq 10. However, Figure 6 shows that confining the redox centers within a dense supramolecular assembly makes the reaction entropy even more sensitive to the ionic charge.

This observation could be related to the solvent content of the spontaneously adsorbed monolayer. The magnitude of the intercept of plots, such as those illustrated in Figure 6, is related to the solvent acceptor number and has been interpreted in terms of disruption of the internal solvent structure by the charged species. That an intercept of zero is observed for the monolayer

(28) Hupp, J. T.; Weaver, M. J. *J. Phys. Chem.* **1984**, *88*, 1860.
(29) Barr, S. W.; Guyer, K. L.; Li, T. T.-T.; Liu, H. Y.; Weaver, M. J. *J. Electrochem. Soc.* **1984**, *131*, 1626.
(30) Noyes, R. M. *J. Am. Chem. Soc.* **1962**, *84*, 513.

system suggests that the effective solvent acceptor number within the film is close to that found in bulk acetonitrile solution. This conclusion supports the interfacial capacitance data discussed previously which suggested that the interior of the monolayer is highly solvated. The difference between the bound and free systems could be due to steric congestion in the monolayer, which may inhibit complete insertion of charge-compensating counterions, thus causing increased polarization around the redox center and a higher reaction entropy. However, it is interesting to speculate as to the effect of the electric field in the two situations. In the case of the spontaneously adsorbed monolayer, the close packed structure and perhaps a lower dielectric constant may cause a higher electric field strength to be experienced by the bound centers.[8c] This could induce greater solvent ordering causing a higher reaction entropy to be observed.

Temperature Dependence of *k*. The activation enthalpy extracted from an Arrhenius plot of ln k vs T^{-1} measured at a constant potential has been termed "ideal"[31] and it is labeled here as $\Delta H_I^{\ddagger}$. For a reduction or cathodic reaction, this electrochemical activation enthalpy can be separated into a "chemical" activation enthalpy term, $\Delta H^{\ddagger}$, and a contribution from the "electrical" driving force, $\alpha_c F\phi_m$, where ϕ_m is the Galvani potential which corresponds to the formal potential of the reaction under consideration at a given temperature, according to

$$\Delta H_{I,e}^{\ddagger} = -R \left.\frac{\partial \ln k}{\partial\left(\frac{1}{T}\right)}\right|_{\phi_m} = \Delta H^{\ddagger} - \alpha_c F\phi_m \qquad (11)$$

The temperature dependence of the heterogeneous electron transfer rate has been investigated using temperature-resolved chronoamperometry over the range −5−40 °C. An overpotential of 100 mV, as determined at 298 K, was used throughout these experiments, and the resulting current−time transients were similar to those illustrated in Figure 3. The corresponding semilog plots were linear over approximately 1−5 lifetimes, and the heterogeneous electron transfer rates were evaluated from the slopes. In a typical set of experiments, the temperature was systematically varied over a range and then returned to the initial temperature. The same slope, $-k$, and intercept, ln(kQ), were observed within experimental error for the initial and final transients. This consistency indicates that cycling the temperature does not change the heterogeneous kinetics or the quantity of material immobilized on the electrode surface. The heterogeneous electron transfer rate increases with increasing temperature as anticipated for a thermally activated process. As illustrated in Figure 7, Arrhenius plots of ln k vs T^{-1} are linear ($R^2 > 0.995$) over the temperature range −5 to 40 °C. Table 2 contains the activation enthalpies, $\Delta H^{\ddagger}$, obtained from the slopes of these plots after using the experimental transfer coefficient to correct for the electrical driving force (100 mV) according to eq 11. These data indicate that the activation enthalpies for the 3+/2+, 2+/1+, and 1+/0 processes are significantly different with values of 43.1 ± 2.8, 31.9 ± 2.2, and 25.8 ± 1.9 kJ mol^{-1}, being observed for the metal- and two ligand-based reactions, respectively.

In principle, it is possible to use the experimental enthalpies and entropies of activation to calculate free energies of activation. Comparing these values with the value of the reorganization energy provided by Finklea and Hanshew's model is an important test of consistency between these two independent approaches. The cathodic free energy of activation has been calculated according to eq 12:[8a,32]

$$\Delta G_c^{\ddagger} = \Delta H_{I,c}^{\ddagger} - T\alpha_c \Delta S_{rc}^{\circ} \qquad (12)$$

and Table 2 contains the data. These data show that, for the three redox processes investigated, $\Delta G_c^{\ddagger}$ and $\lambda/4$ agree to within 10%.

Preexponential Factor. That $\Delta G_c^{\ddagger}$ depends on the particular redox couple being probed is significant. This result emphasizes the importance of considering reorganization energy effects when attempting to use rate data to probe the degree of electronic coupling between remote redox sites and the electrode surface. Table 2 contains values of A_{et} ($\equiv \kappa_{el}\nu_n$) that have been determined using the experimental values of $\Delta G_c^{\ddagger}$ and k°. One might expect that the electronic transmission coefficient would be significantly larger for those situations where mediating electronic states within the bridging ligand play an important role in dictating the overall heterogeneous electron transfer rate.[7a] Therefore, an important aim is to calculate κ_{el} from the experimental preexponential factor. Where the electron transfer reaction features a sharp barrier top as expected for weak donor/

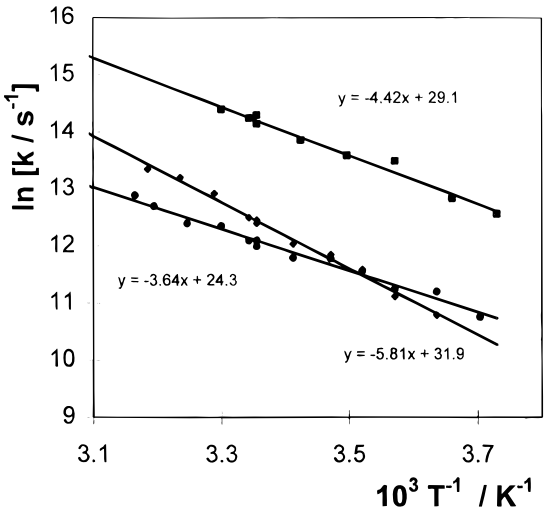

Figure 7. Arrhenius plots of ln k vs T^{-1} for a [py(p3p)] monolayer. The heterogeneous electron transfer rate constant was measured at an overpotential of 100 mV determined at 298 K. From top to bottom, on the left-hand side, the data are for the 2+/1+, 3+/2+, and 1+/0 redox couples, respectively. The electrolyte is 0.2 M $TBABF_4$ in acetonitrile. The errors in the rate constants are approximately equal to the size of the symbols.

Table 2. Activation Parameters and Preexponential Factors for Metal- and Ligand-Based Electron Transfer Reaction within [py(p3p)] Monolayers[a]

charge	λ, kJ mol^{-1}	$\Delta H^{\ddagger}$, kJ mol^{-1}	$\Delta G_c^{\ddagger}$,[b] kJ mol^{-1}	$10^{-6}A_{et}$,[c] s^{-1}	$10^6\kappa_{el}$
3+/2+	48	43.1(2.8)	11.5(0.8)	4.6(1.4)	1.5(0.7)
2+/1+	62	31.9(2.2)	14.2(1.2)	77.3(8.4)	22.9(8.3)
1+/0	80	25.8(1.9)	19.8(1.3)	97.9(8.6)	24.4(9.9)

[a] Numbers in parentheses represent the standard deviations for at least three individual monolayers. Supporting electrolyte is 0.2 M $TBABF_4$ in acetonitrile. [b] Free energy of activation determined from the cathodic ideal electrochemical enthalpies as measured from the temperature dependence of the heterogeneous rate constant and the reaction entropy, ΔS_{rc}°. [c] Preexponential factor extracted from the standard heterogeneous electron transfer rate constant using $\Delta G_c^{\ddagger}$.

(31) (a) Li, T. T.-T.; Guyer, K. L.; Barr, S. W.; Weaver, M. J. *J. Electroanal. Chem.* **1984**, *164*, 27. (b) Yee, E. L.; Weaver, M. J. *Inorg. Chem.* **1980**, *19*, 1077.

(32) (a) Weaver, M. J. *J. Phys. Chem.* **1979**, *83*, 1748. (b) Weaver, M. J. *J. Phys. Chem.* **1976**, *80*, 2645.

acceptor electronic coupling, a dielectric continuum treatment predicts that the nuclear frequency factor, ν_n, is given by eq 13,[24a,33]

$$\nu_n = \tau_l^{-1} (\Delta G_c^{\ddagger}/(4 \pi k_B T))^{1/2} \quad (13)$$

where τ_l^{-1} is the inverse longitudinal relaxation time for acetonitrile (3.3 ps^{-1}). This model is most appropriate for adiabatic reactions involving short electron transfer distances and relatively strong electronic coupling between the reactants. In contrast, the frequency factor for nonadiabatic reactions is not expected to depend on the relaxation time of the solvent but instead depends on square of the electronic coupling matrix element, H_{12}. Previous investigations into the effects of solvent on the heterogeneous electron transfer rates in this system have demonstrated that, while the electron transfer reaction is nonadiabatic, the electron transfer dynamics depend strongly on the longitudinal relaxation time of the solvent. Therefore, eq 13 has been used to estimate ν_n for each of the three redox couples investigated. These values have then been used to estimate κ_{el} from the experimental preexponential factors. Table 2 shows that for both metal-based oxidation and ligand-based reduction the electronic transmission coefficients are considerably less than unity. This observation indicates that there is a low probability of electron transfer once the nuclear transition state has been attained, suggesting a nonadiabatic reaction involving weak coupling between the metallic states of the electrode and the localized orbitals of the redox center.[22a] However, the magnitude of κ_{el} is distinctly different for the metal- and ligand-based redox reactions with κ_{el} increasing from $(1.5 \pm 0.7) \times 10^{-6}$ for the metal-based reaction to $(23 \pm 8) \times 10^{-6}$ for the first ligand-based reduction reaction.

There are a number of reasons that could cause κ_{el} to be different for the bpy-based reactions compared to the metal-based processes. For example, the orientation of the adsorbate on the electrode surface may be such that the electron transfer distance is shorter for the ligand-based redox reactions. Indeed, this orientation may be potential dependent since the formal potential for the $Os^{2+/3+}$ redox reaction is positive of the potential of zero charge (pzc), while those of the bpy-based reactions are negative of the pzc. However, the data presented in Figure 4 suggest that while redox switching of the bpy ligands proceeds via a through-bond mechanism, through-space electron tunneling is the dominant pathway for metal-based reactions. These electronic transmission data are consistent with this result and suggest that a superexchange pathway which is both symmetry and energy favorable exists for the bpy-based redox reactions.

(33) Morgan, J. D.; Wolynes, P. G. *J. Phys. Chem.* **1987**, *91*, 874.

Conclusions

The adsorbed monolayers considered here exhibit nearly ideal electrochemical responses as the potential, temperature, and experimental time scale are varied over a wide range. Chronoamperometry has been used to probe the rate of heterogeneous electron transfer across the monolayer/microelectrode interface. This process can be characterized by a single rate constant at high electrolyte concentrations suggesting that heterogeneous electron transfer across these metal/monolayer interfaces is mechanistically uncomplicated. This unusual ideality has allowed the nature of the activation barrier to electron transfer and the degree of electronic coupling between the remove redox centers and the microelectrode to be probed in considerable detail. Measurements of the potential dependence of the heterogeneous electron transfer rate constant, *k*, suggest that for the ligand-based reductions electron transfer occurs via a through-bond tunneling mechanism, while electron transfer to the metal center proceeds via a through-space tunneling mechanism. These observations are consistent with mediating electronic states within the bridging ligand (superexchange) being important only for the ligand-based reductions where the orbital energies of the acceptor sites and the bridging ligand are similar.

Acknowledgment. R.J.F gratefully acknowledges Professor Larry R. Faulkner of the University of Illinois at Urbana—Champaign for the generous loan of the high-speed potentiostat used in this work. Financial support from Forbairt, the Irish Science and Technology Agency, under Basic Research Grant SC/95/209 is gratefully acknowledged. The generous loan of potassium hexachloroosmate(IV) by Johnson Matthey under the loan scheme is deeply appreciated.

IC951343E